Lab on a Chip

Accepted Manuscript

ROYAL SOCIETY OF CHEMISTRY

www.rsc.org/loc

Lab on a Chip

RSCPublishing

TUTORIAL REVIEW

The promise of microfluidic artificial lungs

Cite this: DOI: 10.1039/xoxxoooooox

Joseph A. Potkay[a]

Received ooth July 2014,
Accepted ooth January 2014

DOI: 10.1039/xoxxoooooox

www.rsc.org/

Microfluidic or microchannel artificial lungs promise to enable a new class of truly portable, therapeutic artificial lungs through feature sizes and blood channel designs that closely mimic those found in their natural counterpart. These new artificial lungs could potentially: 1) Have surface areas and priming volumes that are a fraction of current technologies thereby decreasing device size and reducing the foreign body response; 2) Contain blood flow networks in which cells and platelets experience pressures, shear stresses, and branching angles that copy those in the human lung thereby improving biocompatibility; 3) Operate efficiently with room air, eliminating the need for gas cylinders and complications associated with hyperoxemia; 4) Exhibit biomimetic hydraulic resistances, enabling operation with natural pressures and eliminating the need for blood pumps; and, 5) Provide increased gas exchange capacity enabling respiratory support for active patients. This manuscript reviews recent research efforts in microfluidic artificial lungs targeted at achieving the advantages above, investigates the ultimate performance and scaling limits of these devices using a proven mathematical model, and discusses the future challenges that must be overcome in order for microfluidic artificial lungs to be applied in the clinic. If all of these promising advantages are realized and the remaining challenges are met, microfluidic artificial lungs could potentially revolutionize the field of pulmonary rehabilitation.

A. Introduction

Lung disease afflicts more than 235 million people worldwide and kills more than 3 million people annually [1]. In the United States, more than 35 million Americans are living with chronic lung disease; it is responsible for nearly 400,000 deaths every year and is currently the only major disease with an increasing death rate [2]. Acute respiratory distress syndrome (ARDS) has a mortality rate between 25 and 40% and afflicts 200,000 Americans each year [2].

In the clinical setting, positive pressure ventilation has been traditionally used to partially compensate for the pulmonary insufficiency caused by lung disease. However, the high airway pressures and oxygen concentrations can result in barotrauma, volutrauma, and biotrauma, and can exacerbate the original illness, even resulting in multi-organ failure [3]. Artificial lung technologies have been developed to provide respiratory support without the drawback of ventilator-induced injury. In acute cases, artificial lung technologies enable the natural lung to heal while the patient rehabilitates. In chronic cases, artificial lungs may serve as a bridge to transplant or eventually as a fully artificial replacement for the natural lung, increasing survival and improving quality of life. The CESAR study recently demonstrated that extracorporeal membrane oxygenation (ECMO – a procedure that uses an artificial lung and blood pump to achieve cardiopulmonary support) provided a significantly improved survival rate (63% vs. 47%) for patients with severe acute respiratory failure when compared to patients treated with mechanical ventilation [4].

Artificial lung technologies can be grouped into four categories: extracorporeal, paracorporeal, intrathoracic, and intravenous artificial lungs. Some of these devices have undergone human clinical trials [5, 6]. However, only extracorporeal membrane-based artificial lungs are currently clinically used, predominantly during cardiopulmonary bypass and less frequently for respiratory failure or as a bridge to lung transplant [7, 8]. The Maquet Quadrox represents the state-of-the-art in commercially-available artificial lung technologies [9]. The Quadrox has a low pressure drop and is capable of being driven by the natural heart in some clinical applications. A single Quadrox has been used clinically for up to two months with systemic anticoagulation [10]. The Quadrox has recently been used for ambulatory ECMO in which the artificial lung, blood pump, computer, battery, and oxygen cylinder can be mounted to a wheeled pole to provide limited mobility in the ICU setting [11, 12, 13].

Despite tremendous advancements, treatment and outcomes with artificial lung systems remain less than optimal. Current systems only permit minimal ambulation and their use is typically limited to the ICU. Truly portable systems that enable

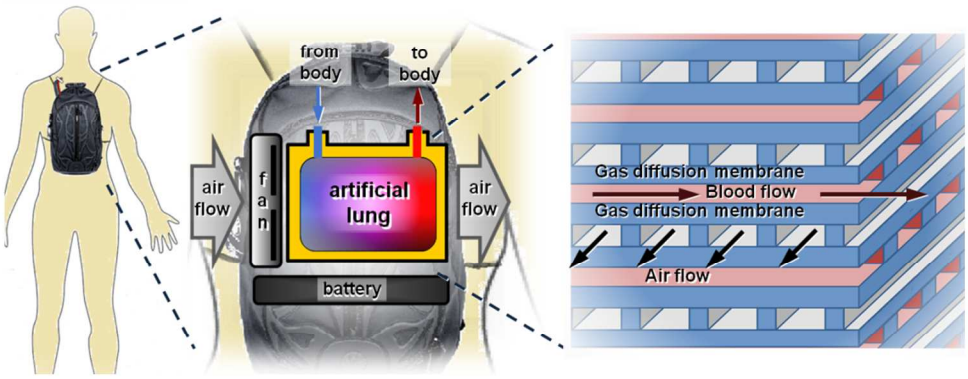

Fig. 1 A conceptual drawing of an initial clinical application of microfluidic artificial lung technology – an ambulatory pumpless extracorporeal lung assist system.

full ambulation are simply not possible with current technologies. Further, device-mediated complications including inflammation, device clotting, and hemolysis are common during treatment with current systems, especially in longer cases. Most devices have clinical lifetimes measured in days and require systemic anticoagulation. Finally, current systems are only capable of supporting the respiratory needs of a patient at rest. Thus, for artificial lungs to realize their potential for both long term respiratory support and more effective short term rehabilitation, significant improvements in biocompatibility, gas exchange, and portability must be made [8].

Microfluidic artificial lungs have the potential to provide drastically improved pulmonary support through three means: 1) Improved gas transfer performance compared to current devices to enable complete, ambulatory respiratory support of active patients, 2) Increased biocompatibility to increase device lifetime, decrease anticoagulation, enable long-term treatment, and increase patient health, and 3) Increased portability to enable truly ambulatory care and improved patient quality of life. A conceptual drawing of one possible initial clinical implementation of microfluidic artificial lung technology is shown in Fig. 1. The device is mounted on the chest or back and vascular access is achieved via the subclavian artery and vein (AV) to permit ambulation. Blood flow is driven by the natural heart and the supply gas (air) is delivered by a battery-driven fan integrated into the system. Should more oxygen exchange be required by the patient, a venovenous (VV) configuration (i.e. a vein to vein connection) could be used with blood flow driven by a small pump (e.g. the Abiomed Impella).

Section B of this manuscript describes advantages of microfluidic artificial lungs (relative to current hollow fiber technology) that should be achievable based on evidence in the literature and current technology. Section C justifies these potential claims by deriving the performance and scaling limits of microfluidic artificial lungs using a verified mathematical model. Section D discusses additional important design considerations for microfluidic artificial lungs including blood flow network design, hemocompatible coatings, pressure drop and shear, and choice of supply gas. Section E describes the current state of research in this growing field and details which of the potential benefits of microfluidic artificial lungs described in Section B have already been realized. Section F concludes the manuscript by detailing current hurdles to achieving microfluidic artificial lung systems for human use.

B. The Promise of Microfluidic Artificial Lungs

A microfluidic or microchannel artificial lung is an artificial lung in which the smallest features, including blood channel diameter and membrane thickness, are between 1 and 100 μm, or similar in size to the smallest features in the natural lung. Microfluidic artificial lungs are formed using microfabrication techniques that allow the precise control of not only minimum feature sizes, but also of the blood flow path. Microfabrication and microtechnology can thus be used to create microfluidic artificial lungs with feature sizes similar to those in the natural lung as well as containing blood flow paths that closely mimic those found in their natural counterpart. These two properties have enormous implications in terms of the gas exchange, portability, and biocompatibility of artificial lungs, as described in more detail in the subsections below.

B.1. Current artificial lung technology

In order to understand the benefits of microfluidic artificial lungs, it is first helpful to take a look at current artificial lung technology. Artificial lungs mimic the function of natural lungs by adding oxygen to and removing carbon dioxide from the blood. Nearly all current commercially-available artificial lungs use hollow-fiber technology. A representative device implementing this technology, the Maquet Quadrox, is displayed in Fig. 2. During operation, a blood pump drives blood flow from the body and through the device (Fig. 2A). Blood enters the base of the device, flows vertically up its side and then transversely through a dense bundle of hollow fibers (Fig. 2B). Each hollow fiber (typically made from polypropylene or polymethylpentene) is microporous and highly permeable to both carbon dioxide (CO_2) and oxygen (O_2). Blood flows along the outside of each hollow fiber and the sweep gas (typically pure O_2) flows inside of the fiber (Fig.

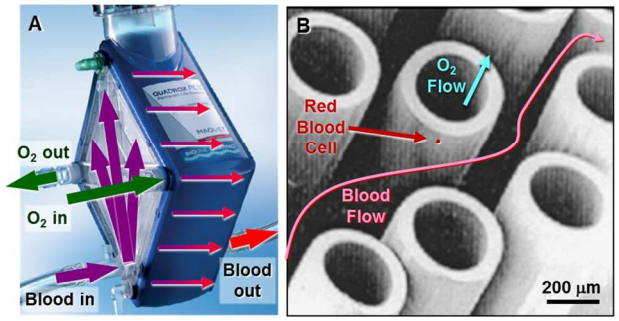

Fig. 2 Current hollow-fiber artificial lung technology. A. Diagram of the Maquet Quadrox [9]. B. Cross-section of the gas diffusion interface in hollow-fiber artificial lungs (modified from [43]).

2B). Oxygen is transferred into the blood and CO_2 out of the blood by diffusion through the wall of the hollow fibers (the membrane). Blood flows through the fiber bundle in a circuitous path that creates mixing and enhances gas transfer (Fig. 2B). An integrated heat exchanger can heat or cool the blood, which is then returned to the body. This predominant artificial lung design has a number of drawbacks which are potentially addressed through microfluidic artificial lung technology, as described in detail below.

B.2. Gas exchange

The performance of current artificial lungs is significantly lower than that of their natural counterpart. The human lung provides a maximum gas exchange rate for both O_2 and CO_2 of 2-6 L/min [8] utilizing air as the supply gas. In contrast, current artificial lungs are only capable of a maximum gas exchange rate of 250-400 ml/min [8] using pure oxygen (stored in gas cylinders) as the supply gas. Current artificial lungs are thus only suitable for the short-term respiratory support for patients at rest. This gas exchange insufficiency is due to the smaller surface area, smaller surface-area-to-volume ratio, greater membrane thickness, and larger blood channel heights of artificial lungs compared to the human lung [8].

Through the use of microfabrication techniques, it is possible to create artificial lungs with feature sizes that are, for the first time, similar to those in the natural lung. Figure 3 compares the size scale of the units of gas exchange in the natural lung and a microfluidic artificial lung. For comparison, Fig. 2B shows the unit of gas exchange in a conventional artificial lung. In microfluidic artificial lungs, smaller blood channel diameters and membrane thicknesses result in drastically reduced diffusion distances for O_2 and CO_2 transferring between blood and the sweep gas. Reduced diffusion distances result in an increase in gas exchange efficiency. Larger gas exchange efficiencies will ultimately result in larger gas exchange for a fixed membrane area, thereby potentially enabling respiratory support for active patients.

B.3. Priming volume

Priming volume is the amount of blood required (external to the body) to fill or prime an artificial lung and its blood circuit. The priming volume is thus the amount of blood that is being exposed to an artificial surface at any given moment. Reducing the priming volume of artificial lung circuits during cardiopulmonary bypass procedures has been shown to reduce post-operative blood transfusions, advance patient hemodynamic recovery, and increase hematocrit values during the procedure [14, 15, 16]. Although artificial lung manufacturers have made significant progress toward reducing priming volume, adult devices still have priming volumes near or in excess of 200 ml [9, 17, 18, 19].

Microfluidic artificial lungs harness small artificial capillaries and thin gas exchange membranes in order to achieve improved gas exchange efficiency and very high surface-area-to-volume (SAV) ratios. The combination of large gas exchange efficiency and high surface-area-to-volume ratio can be used to produce an artificial lung with a very small blood volume for a given gas exchange rate. Priming volumes of microfluidic artificial lungs promise to be a fraction of that in current devices, thereby potentially improving rehabilitation from lung disease or after cardiopulmonary bypass procedures. In general, the priming volume of microfluidic artificial lungs should be minimized as much as possible in order to minimize the foreign body response. However, at some point, the blood circuit and the manifold that deliver blood to the microchannels will dominate the total priming volume thus mitigating the benefit of minimizing the priming volume of the artificial lung further. Depending on the application and length of tubing in the blood circuit, the blood circuit and manifold may have a priming volume as small as 50 ml or up to or exceeding 500 ml.

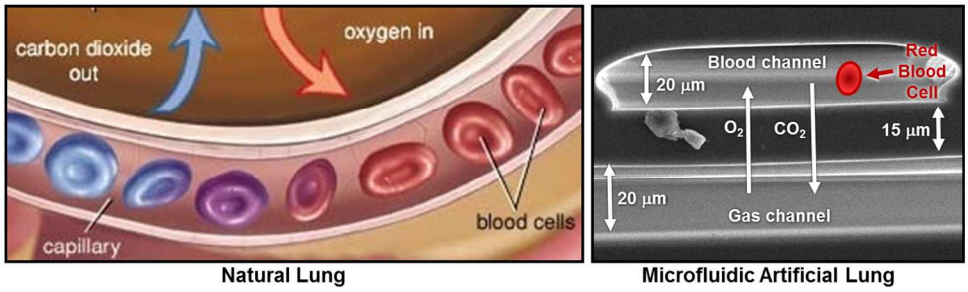

Fig. 3 A comparison of the size of the basic unit of gas exchange in the natural lung [80] and microfluidic artificial lungs. Red blood cells in each figure serve as a size reference.

B.4. Hydraulic resistance

Most commercially-available artificial lungs have large blood-side hydraulic resistances, or large pressure drop to blood flow ratios. These large hydraulic resistances necessitate the use of a blood pump and preclude operation using only naturally-available pressures. A blood pump not only limits portability due to its size and weight, but also adds pro-coagulatory effects and can result in blood cell damage, including hemolysis [20]. Blood pumps should thus be avoided when the application permits. There are commercially-available [18] and research [21, 22] devices that have been designed to have a low blood-side hydraulic resistance, thereby enabling pumpless extracorporeal lung assist (PECLA) applications.

During the construction of microfluidic artificial lungs, photolithography and microfabrication enable the creation and design of virtually any desired two-dimensional blood flow path. These custom blood flow paths can thus be designed to have small hydraulic resistances, thereby enabling operation with naturally available pressures and avoiding the use of blood pumps that limit portability and blood compatibility.

Depending on the application, the required pressure drop (and thus hydraulic resistance) for an artificial lung may vary. Two examples are provided here. For a peripheral artery-to-vein (arteriovenous) connection, the difference between the mean arterial and venous pressures in a normal adult is approximately 80 mmHg [23]. For an artificial lung connected in parallel with the natural lungs, the pressure drop between the pulmonary artery and left atrium is approximately 10 mmHg [23]. These two values thus provide upper and lower bounds for the working pressures of microfluidic artificial lungs systems, depending on the application.

B.5. Biomimetic flow networks

Current artificial lungs consist of hundreds to thousands of hollow fiber tubes that are bundled tightly together (Fig. 2). Blood flows between the fibers in a tortuous path that enhances mixing and, thus, gas exchange. However, as is apparent in Fig. 2b, the dimensions along this tortuous flow path are non-uniform, resulting in areas of high flow and stasis. Areas of high flow correspond to increased shear stress on cells and platelets. Elevated shear stresses can activate platelets (as low as 12 to 15 dyn/cm^2 in a few specific experiments) and large shear stresses can lyse red blood cells [24, 25, 26]. Areas of low flow and stasis promote thrombus initiation [27]. Flow non-uniformity and stasis also create inefficiencies in the gas exchange process.

As mentioned previously, microfluidic artificial lungs can be designed with virtually any desired two-dimensional blood flow path. Researchers have used this ability to create blood flow networks that follow scaling and branching laws and shear stresses in the natural lung [27, 28]. These microchannel networks can be designed such that cells and platelets experience pressures, shear stresses, and branching angles that copy those in the body. It is believed that by mimicking the physiological properties of real vessels, the blood flow paths in microfluidic artificial lungs will have improved biocompatibility and lifetime compared to their conventional counterparts.

B.6. Membrane technology

Polypropylene (PP) hollow fiber membranes (Fig. 2) are the core technology of today's commercially-available artificial lungs. These hollow fibers are highly permeable to oxygen and carbon dioxide due to their micro-porosity. This porosity can result in unwanted air leakage and can cause membrane performance to degrade over time due to blood plasma leakage into the pores [8]. In polymethylpentene (PMP) hollow fiber devices, plasma leakage does not occur, but air leakage through the membrane is still a potential danger [29].

Microfabrication enables the creation of extremely thin, highly permeable non-porous polymer membranes. These thin, non-porous membranes can achieve excellent gas transfer and avoid the drawbacks of hollow fiber technologies. Specifically, the lifetime and performance of non-porous membranes will not degrade over time due to due to plasma leakage. In addition, non-porous membranes eliminate the complication of gas leakage that is possible in current technologies [8, 29].

B.7. Mechanical compliance

The hollow fibers in current artificial lungs (Fig. 2) are rigid and do not deflect with changes in blood pressure. Microfluidic artificial lungs can employ thin, flexible, polymer membranes that are mechanically similar to the blood-gas membrane in the natural lung. Just as pulmonary capillaries expand and contract with changes in pulmonary blood pressure, the height of the microchannels in microfluidic artificial lungs can vary with changes in blood pressure if they contain thin, flexible membranes. The mechanical compliance of microfluidic artificial capillaries thus promises to more closely mimic that in the natural lung (as compared to current artificial lung technologies). This property is expected to result in a more natural hydraulic resistance and a more natural environment for cells and platelets. The drawbacks of compliant membranes are that they could lead to occlusion, clotting, and transient pressure changes. Devices implementing compliant membranes will thus need to be designed carefully to mitigate these potential issues.

B.8. Supply gas

Currently-available artificial lungs typically require pure oxygen as the supply gas during normal use. The use of pure oxygen has several drawbacks. First, pure oxygen is stored in (bulky) gas cylinders, thereby limiting patient mobility and quality of life. Next, in conventional artificially lungs using pure oxygen, it has been shown that oxygen-derived free radical generation may be increased, potentially resulting in oxygen toxicity issues [30, 31]. Further, hyperoxemia (high oxygen content in blood) has been associated with increased mortality and can increase platelet activation, aggregation, and thrombosis through increased generation of reactive oxygen

species [32]. These factors can negatively impact clinical outcomes and device lifetime.

Microfluidic artificial lungs can operate using air as the supply gas due to their high gas exchange efficiency. Use of air as the supply gas promises to provide more natural ventilation to patients and eliminate the potential complications of using pure oxygen. Finally, the use of air as the supply gas has large implications in terms of portability. Instead of using pure O_2 stored in bulky gas cylinders, microfluidic artificial lungs will potentially operate using air supplied by light weight, battery powered fans (for an extracorporeal system) or perhaps by eventually by tapping into the natural air circulation (for future implantable systems).

B.10. A potential disadvantage

One potential disadvantage of microfluidic artificial lungs is related to the size of their blood channels. The diameter or height of the artificial capillaries in microfluidic artificial lungs is one design parameter that can be varied. In some cases, these blood channels have been designed to be on a size scale similar to those in the human lung and channels down to 10 μm in diameter have been demonstrated [33]. When the foreign body response and clotting cascade are initiated, thrombus formation can quickly block the miniature channels and reduce the device's operational lifetime. Uncoated microfluidic artificial lungs with small diameter microchannels have been shown to clot in less than one hour of operation with heparinized whole blood [33, 34, 35]. However, with appropriate biomimetic blood channel design, blood compatible surface coatings, and other strategies (see D.2 and F.2, below), it is hoped that activation of the clotting cascade can be minimized, resulting in small diameter microchannel devices with lifetimes suitable for clinical applications.

B.11. Summary of benefits

Microfluidic artificial lungs thus have the ability to: a) Increase total gas exchange to enable respiratory support for active patients; b) Improve portability by eliminating gas cylinders and pumps and integrating heaters and sensors directly into the device; and, c) Improve biocompatibility and lifetime by providing biomimetic blood flow paths, reducing priming volume, eliminating air and plasma leakage, and reducing the potential for complications due to hyperoxemia. These advancements have the potential to vastly improve clinical outcomes and patient quality of life. The next section investigates the performance and scaling limits of microfluidic artificial lungs.

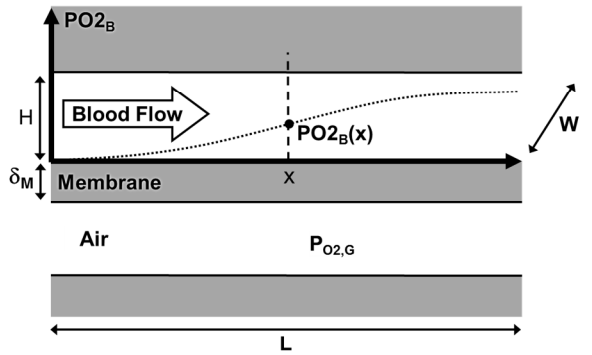

Fig. 4 A side-view drawing of an artificial capillary and gas exchange membrane in a microfluidic artificial lung. Relevant parameters for modelling of oxygen transfer are labelled.

C. Performance and Scaling Limits

The previous section described the potential advantages of microfluidic artificial lungs. This section seeks to quantify some of those benefits by investigating the scaling and performance limits of the units of gas exchange (the artificial capillaries) in microfluidic artificial lungs.

C.1. Mathematical model of gas exchange

According to the FDA Guidance for Cardiopulmonary Bypass Oxygenators 510(k) Submissions, the oxygen gas transfer for any artificial lung can be calculated as a function of the blood flow rate (Q), blood oxygen content at the inlet (CvO2), and blood oxygen content at the outlet (CaO2) of the device [36]:

$$\frac{\Delta V_{O2}}{\Delta t} = (CaO2 - CvO2) \cdot Q \qquad (1)$$

Normal human blood has a hemoglobin concentration of 12 g/dl, an oxygen-hemoglobin binding capacity of 1.34 ml O_2 per gram of hemoglobin, and a solubility of oxygen in blood plasma of 0.00314 ml O_2 per deciliter of blood per mmHg [36]. Equation 1 can thus be written as:

$$\frac{\Delta V_{O2}}{\Delta t} = [1.608 \cdot (SO2_o - SO2_i) + 0.0314 \cdot (PO2_o - PO2_i)] \cdot Q \qquad (2)$$

where $SO2_{is}$ and $SO2_o$ are the blood oxygen saturation (in %) at the device inlet and outlet, respectively, $PO2_i$ and $PO2_o$ are the partial pressure of oxygen in blood (in mmHg) at the device inlet and outlet, respectively, Q is blood flow (in L/min), and $\Delta V_{O2}/\Delta t$ is the oxygen gas transfer (in ml/min). Thus, if the oxygen partial pressure and saturation at the inlet and outlet of a device are known, gas exchange can be calculated.

A simple, first order mathematical model for the partial pressure of oxygen in a microchannel artificial lung, $PO2_B$, was derived in [37]. A diagram showing the key parameters in the model is shown in Fig. 4. The model in [37] was derived for a an array of blood channels with a rectangular cross section and for single sided diffusion, but can be applied to devices with other cross sections and to double sided diffusion with simple modifications [37]. Flow was assumed to be uniform throughout the array of blood channels. The partial pressure of oxygen in blood is assumed to only vary along the length of the blood channel. In small diameter blood channels, variations in partial pressure along the width and height of the channel should be small and are neglected [37]. Here, we assume rectangular cross section blood channels and single sided diffusion. The equation for $PO2_B$ in [37] was a function of the distance along the channel, x, and the average blood flow

velocity, v. Since we are only interested in $PO2_B$ at the outlet of the device, we can set $x=L=A/W_{TOT}$, where L is the blood channel length and W_{TOT} is the sum of widths of all gas exchange blood channels. Using $Q=v \cdot W_{TOT} \cdot H$, where Q is the blood flow and H is the blood channel height, we can then write the original equation as a function of A and Q:

$$PO2_{B,o} = PO2_G + \left(PO2_{B,i} - PO2_G\right) e^{-\frac{A}{Q \cdot S_{B,O2} \cdot R_{D,O2}}} \quad (3)$$

$PO2_{B,i}$ and $PO2_{B,o}$ are the partial pressure of oxygen in blood at the inlet and outlet of the device, respectively, $PO2_G$ is the partial pressure of oxygen in the supply gas, A is the surface area available for gas exchange, Q is blood flow, and $S_{B,O2}$ is the average effective solubility of oxygen in the blood sample under test. $R_{D,O2}$ is the effective resistance to the diffusion of oxygen and is approximated as:

$$R_{D,O2} = \frac{\delta_M}{P_{M,O2}} + \frac{H/2}{S_{B,O2} \cdot D_{B,O2}} \quad (4)$$

where δ_M is the thickness of the gas diffusion membrane, $P_{M,O2}$ is the permeability of the membrane to oxygen, H is the average height of the blood channel, and $D_{B,O2}$ is the effective diffusivity of oxygen in the blood sample being tested [37]. The term H/2 represents the average distance oxygen in blood must diffuse to reach the membrane. For normal human blood, as defined by the FDA Guidance for Cardiopulmonary Bypass Oxygenators 510(k) Submissions [36], $S_{B,O2}$ and $D_{B,O2}$ can be estimated to be 7.9×10^{-4} ml O_2 • ml blood^{-1} • mmHg^{-1} and 1.4×10^{-6} cm^2 • s^{-1}, respectively [37]. After oxygen partial pressure is calculated, oxygen saturation ($SO2_i$ and $SO2_o$) can be determined using the Hill equation [38] and gas exchange can be calculated using Equation 2.

C.1.a. Regarding the membrane material

The membrane material for a microfluidic artificial lung should: 1) Have a high permeability to oxygen and carbon dioxide; 2) Be able to be integrated into microfabrication processes; 3) Have adequate mechanical durability; and, 4) Be biocompatible. To date, non-porous and porous polydimethylsiloxane (also known as PDMS or silicone rubber), microporous polycarbonate (PC), and microporous polypropylene (PP) have been used as the membrane material in microfluidic artificial lungs (See E). For the calculations in the current section, we assume that non-porous PDMS is the membrane material. PDMS has a history of use in microfluidic devices and medical implants, has a very high permeability to O_2 and CO_2 (600 and 3250 Barrers, respectively), and has excellent mechanical durability. However, it should be noted that the general trends and scaling laws described below are applicable to membranes of many materials.

C.2. Effect of scaling key feature sizes of artificial capillaries

In this section, the mathematical model presented above is used to determine the impact that miniaturizing both the blood channel height and membrane thickness of the artificial capillaries have on the performance of microfluidic artificial lungs. A common metric used to compare the performance of artificial lungs is termed the device's "rated flow". The rated flow of an artificial lung is defined as the maximum blood flow rate at which an inlet blood saturation of 70% can be oxygenated to an outlet oxygen saturation of 95% [8]. Rated flow is thus a simple and direct measure of the both the gas exchange and blood flow capacity of an artificial lung. To determine rated flow, Equation 3 can be solved for flow to give:

$$Q = \frac{A}{S_{B,O2} \cdot R_{D,O2} \cdot ln\left(\frac{PO2_{B,i} - PO2_G}{PO2_{B,o} - PO2_G}\right)} \quad (5)$$

Using the Hill equation [38] and assuming normal human blood, the inlet and outlet partial pressure can be calculated that correspond to oxygen saturations of 70% and 95% ($PO2_{B,i}$ =

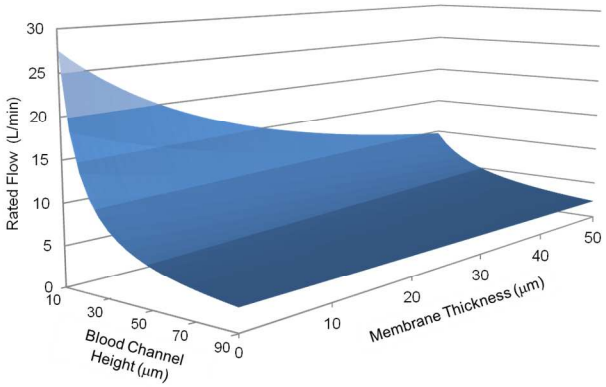

Fig. 5 A theoretical plot showing the impact of a microfluidic artificial lung's membrane thickness and blood channel height on its rated blood flow. The vertical axis displays the rated blood flow of a microfluidic artificial lung with a surface area of 1 m^2 while using pure O_2 as the supply gas. The plot was generated using the mathematical model described in [37]. PDMS is assumed to be the membrane material.

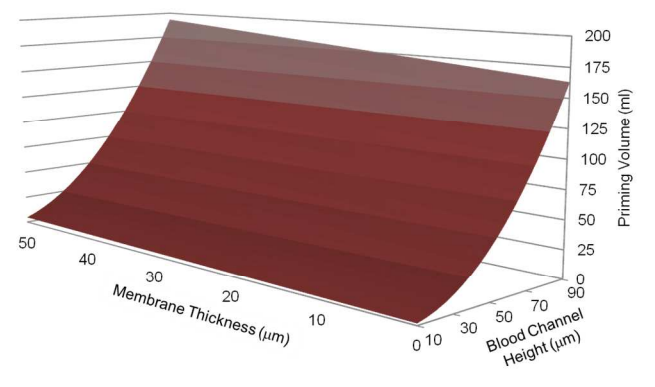

Fig. 6 A theoretical plot showing the impact of a microfluidic artificial lung's membrane thickness and blood channel height on priming volume. The vertical axis represents the priming volume of a microfluidic artificial lung with the specified membrane thickness and blood channel height and a rated blood flow of 4.5 L/min (using pure O_2 as the supply gas). The plot was generated using the mathematical model described in [37]. The membrane material is assumed to be PDMS.

36.4 mmHg and $PO2_{B,o}$ = 79.2 mmHg). Equation 5 can then be solved to determine the rated flow and plotted for varying values of membrane thickness (δ_M) and artificial capillary height (H) as shown in Fig. 5. Membrane thickness and capillary height affect the rated flow through $R_{D,O2}$ as given in Eqn. 4. As apparent in Fig. 5, both the membrane thickness and artificial capillary height have a large impact on rated flow and thus gas exchange. In fact, to maximize rated flow and gas exchange (for a fixed gas exchange area), both parameters should be minimized as much as is practically possible (see C.2). It is notable that the model predicts that rated flow is a function of the gas exchange area and is not dependent on the ratio of the blood channel length to width.

In order to determine the impact of miniaturization on blood priming volume, blood volume of the artificial capillaries can be calculated as gas exchange area, A, multiplied by the blood channel height, H. The gas exchange area can be determined from Equation 5 for a fixed rated flow, Q. Figure 6 shows the impact that scaling the blood channel height and membrane thickness have on capillary priming volume for a fixed rated blood flow of 4.5 L/min and pure oxygen as the supply gas. This rated flow was chosen because it is comparable to the state-of-the-art commercially-available artificial lungs. Capillary priming volume is proportional to the blood channel height squared and to the first power of the membrane thickness. Thus, once again, it is beneficial to minimize both parameters. It should be noted that the blood volume calculated in Fig. 6 consists only of the blood volume that is contributing to gas exchange. Additional blood volume may be required in microfluidic artificial lungs in order to route blood to the artificial capillaries (see D.1). However, Fig. 6 still demonstrates that scaling the dimensions of artificial lungs can result in dramatically reduced priming volumes.

C.2.a. Design constraints for artificial capillaries

In order to maximize the performance of the units of gas exchange (artificial capillaries) in microfluidic artificial lungs and minimize their priming volume, it is beneficial to minimize their blood channel heights and membrane thicknesses. However, there are practical and physical aspects that limit the design of microchannel artificial capillaries. First and foremost is the physical size of the components of blood. Blood is composed of blood plasma (water, electrolytes, and proteins) and cells (red blood cells, platelets, and white blood cells). Red blood cells (RBCs), or erythrocytes, have an approximate diameter of 8 μm and a concentration of approximately 5 million cells per microliter [39, 40]. White blood cells (WBCs), or leukocytes, have a diameter between 5 and 20 μm and a concentration of 9 thousand cells per microliter [40]. Platelets, or thrombocytes, are 2 to 3 μm in diameter and have a concentration of 300 thousand cells per microliter [40, 41]. All of these components of blood must be able to flow through the microfluidic channels in a microfluidic artificial lung. To complicate the issue, blood cells are mechanically compliant. Red blood cells have been shown to flow through channels as small as 3 μm in diameter [42]. However, it is plausible that such extreme mechanical deformation of blood cells may have a deleterious effect on biocompatibility. The pulmonary capillaries in the natural lung, on the other hand, have a minimum diameter of approximately 10 μm [43]. It is thus likely that 10 μm is the minimum practical diameter for artificial capillaries in a microfluidic artificial lung as well.

Next, the minimum thickness of the gas diffusion membrane will be limited by mechanical considerations. The tensile strength (the maximum stress that a material can withstand before failing) of the material must not be exceeded when the membrane deflects under pressure. To avoid permanent deformation of the membrane, the elastic limit of the material should not be exceeded during operation. To further ensure the durability of the membrane, its tear strength (how well a material resists the growth of any cuts when under tension) should not be exceeded during deflection. For each specific membrane material and structure, stress and force per length in the membrane will need to be calculated at for all expected pressures to ensure that they don't exceed the material's tensile or tear strength. For Sylgard 184 [44], a silicone elastomer and a common microfluidic material, the tensile strength and elastic limit are 6.7 MPa and the tear strength is 2.6 kN/m.

C.3. Performance limits for microchannel artificial capillaries

Equation 5 can be used to calculate the performance limits of microfluidic artificial lungs given the constraints enumerated above. If it assumed that the artificial capillary has a rectangular cross section with a height is 10 μm, that pure O_2 is used as the supply gas, and that the permeability of the membrane does not limit performance, the rated blood flow for a 1 m^2 microfluidic artificial lung can theoretically approach 27 L/min. In such a device, the blood volume of the artificial capillaries will be minimal (< 10 ml) and total priming volume will be dominated by the volume of channels required to route blood to the artificial capillaries and by the blood circuit. For comparison, the Novalung® iLA Membrane Ventilator has a rated flow of 4.5 L/min for a gas exchange area of 1.3 m^2 using oxygen as the supply gas and a priming volume of 175 ml [18].

D. Additional Design Considerations

The previous section looked at the performance limits of microfluidic artificial lungs in terms of gas exchange and priming volume of their artificial capillaries. This section will look at other design considerations that are necessary to fully design and optimize microfluidic artificial lungs.

D.1. Fluidic routing and branching

In Section B, it was noted that one of the main benefits of microfluidic artificial lungs is that, through microfabrication, it is possible to create virtually any two-dimensional blood flow path. This is in direct contrast to commercially-available artificial lungs that use a tortuous path through a hollow fiber

bundle in order to maximize mixing and thus gas exchange (Fig. 2B).

In a microfluidic artificial lung, the blood flow network can generally be divided into two components based on their purpose: the blood distribution network and the gas exchange channels (i.e. the artificial capillaries). In practice, the blood distribution network and gas exchange channels in a microfluidic artificial lung can either be combined into a single structure or designed and implemented separately. In the first approach, a single blood channel height is typically used to implement a blood flow network that achieves both blood distribution and gas exchange. This approach is simple, but can result in large pressure drops if small channel diameters are used. In the second approach, multiple blood channel diameters are used to implement separate blood distribution channels and gas exchange channels. This second approach can achieve small pressure drops and excellent gas exchange efficiency via small diameter artificial capillaries, but extra area is required for the blood distribution network (which may not contribute to gas exchange significantly).

Whether it is integrated with or separate from the gas exchange channels, an ideal blood distribution network should: 1) Efficiently transport blood with minimal work; 2) Enable operation with natural pressures; 3) Provide uniform (and physiological) flow and shear stress; and, 4) Provide maximum hemocompatibility. Using engineering principles, many designs are possible which will meet these interrelated criteria. In fact, an optimal design for long-term microfluidic blood networks has not yet been experimentally determined. However, since blood cells are used to operating within the natural vasculature, an optimal microfluidic blood network will likely mimic its natural counterpart in terms of the pressures and shear stresses that cells experience.

In 1926, Murray described the branching nature of the mammalian vasculature using the principle of minimum biological work [45, 46]. The result was that simple mathematical equations can be used to describe the relationship between parent and daughter vessels in terms of both radii and branching angles. Since the original publications, Murray's law has been generalized and investigated in more detail [47, 48, 49]. In 1981, Sherman proved that systems following Murray's law use large vessels to minimize the work required to transport blood across large distances and small vessels to minimize diffusion distances and maximize area [48]. Sherman also derived that that fluidic systems following Murray's law will also have a constant shear stress at the vessel wall in all vessels in the system, thereby eliminating areas of high shear stress and stasis [48].

In order to minimize work and maximize efficiency, one possible solution is a blood transporting microfluidic network that implements Murray's law. Such a network would consist of larger microfluidic channels that branch into smaller and smaller channels and ultimately into artificial capillaries. The goal of the large channels is to efficiently deliver blood to the artificial capillaries. The goal of the artificial capillaries is to maximize gas exchange. The relationship between the radii of parent and daughter channels as well as their branching angles should follow Murray's law to the greatest extent possible in order to minimize work (minimize pressure for a given flow). Adherence to Murray's law will also ensure uniform blood flow and shear stress throughout the flow network. However, even if Murray's law is strictly followed, a number of branching configurations are possible.

D.2. Blood compatible materials and coatings

As discussed in Section C, the main disadvantage of microfluidic artificial lungs is that, due to the small size of their artificial capillaries, when the clotting cascade is initiated, thrombus formation can quickly block the microchannels resulting in device failure. For this reason, materials, coatings, and other strategies to improve hemocompatibility will be critical for the long-term operation of microfluidic artificial lungs.

In current clinically-used hollow-fiber artificial lungs and extracorporeal circuits, two main coatings – heparin and poly-2-methoxyethylacrylate (PMEA) - have historically been used to improve hemocompatibility. Both heparin and PMEA-coated devices have exhibited reduced thrombogenicity, reduced platelet adhesion and activation, and reduced inflammation compared to uncoated controls [50]. Heparin-bonded devices and circuits have further been shown to improved post-operative lung function, reduce device failure, reduce the length of hospital stays, reduce required anticoagulation, and reduce bleeding and complications [51]. However, despite these tremendous advancements, current devices are still far from a natural, hemocompatible interface. Device lifetimes are measured in days and device-mediated complications are common during treatment with current artificial lung systems.

For microchannel devices, similar coating strategies will be required to reduce surface protein adhesion and diminish platelet activation. A full discussion of strategies to improve the hemocompatibility of artificial materials has been discussed previously [52, 53, 54]. Recent work on improving the hemocompatibility of microchannel networks is described below in Section E.1.

D.3. Pressure drop and shear stress of artificial capillaries

In Section C, gas exchange in microfluidic artificial lungs was described as a function of the surface area of the artificial capillaries. The equations in Section C can thus be used to design a microfluidic artificial capillaries with specific artificial capillary height, H, membrane thickness, δM, and gas exchange area, A, in order to achieve a targeted rated blood flow (or corresponding oxygen exchange rate). Once the gas exchange area is chosen to achieve a desired rated flow, the dimensions of each artificial capillary can be designed to meet requirements for pressure drop and shear stress. Figure 7 displays the general relationship between the artificial capillary length and the capillary pressure drop and shear stress for a fixed gas exchange area in artificial capillaries with a rectangular cross section. Pressure drop is typically a linear function of channel length ($\Delta P = 12 \cdot \mu \cdot L \cdot W^{-1} \cdot H^{-3}$, where ΔP is the pressure drop, μ is

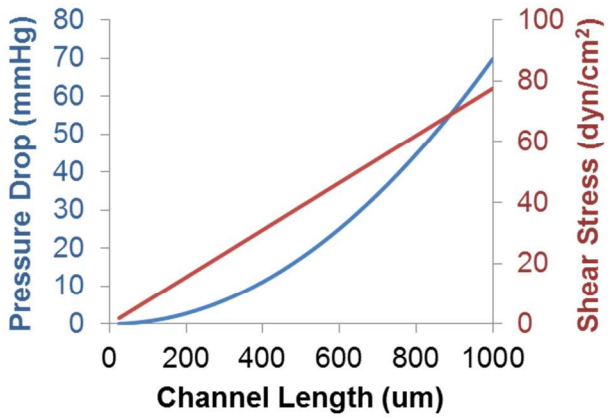

Fig. 7 Pressure drop and shear stress of the artificial capillaries in a microfluidic artificial lung with a 5 μm-thick PDMS membrane, an artificial capillary height of 10 μm, a rated flow of 4.5 L/min, a total gas exchange surface area of 0.25 m^2 and using pure oxygen as the supply gas. The plot shows the trade-off between artificial capillary length and the pressure drop and shear stress in the channels.

viscosity, L, W, and H are length, width and height of the rectangular channel) when channel area is unconstrained. In this case, however, due to the fact that the area is fixed, the total capillary width must decrease as length is increased. This causes the pressure drop to be proportional to the square of the channel length.

In general, artificial capillary length should be chosen to meet the pressure and shear stress requirements of the application. In rectangular channels, shear stress can be estimated as $\tau=\mu \cdot v \cdot H^{-1}$, where τ is shear stress and v is average flow velocity. For blood transport applications, shear stress should likely be chosen to be similar to that in the natural vasculature. In the human vascular system, shear stress ranges between 10 and 70 dyn/cm^2 in arteries and between 1 and 6 dyn/cm^2 in veins [24]. Further, the human body naturally compensates to maintain a mean arterial shear stress between 15 and 20 dyn/cm^2 [24].

D.4. Oxygen versus air as the supply gas

The use of oxygen versus air as the supply gas for future microfluidic artificial lungs entails some interesting trade-offs as shown in Table 1. In the table, two microfluidic artificial lungs, one using pure oxygen and the other using air as the supply gas, were designed using the analysis of Section C and theory developed in [37]. In both cases, the capillary height was fixed at 10 μm (rectangular cross section) and the membrane thickness was fixed at 5 μm. These values were chosen as they represent approximately the minimum practical capillary height and membrane thickness (see C.2, above) and, thus, the best case for maximum gas exchange. In each device, the rated blood flow was set to 4.5 L/min and the capillary pressure drop was fixed at 10 mmHg. A rated blood flow of 4.5 L/min is comparable with current artificial lung technologies. A capillary pressure drop of 10 mmHg is compatible with operation with natural pressures in the peripheral vasculature (see B.4). The capillary gas exchange area of each device was then calculated using Equation 5. With the area known, the capillary blood volume was calculated as the product of area and capillary height. With the area and desired pressure drop known, the required capillary length and associated shear stress were then calculated.

Table 1 Comparison of using air versus pure oxygen as the supply gas for a microfluidic artificial lung. For the comparison, a 5 μm-thick PDMS membrane, 10 μm-tall artificial capillaries were used in all calculations. In addition, rated blood flow and capillary pressure drop were fixed at 4.5 L/min and 10 mmHg, respectively.

Supply Gas	Pure oxygen	Air
Rated Blood Flow (L/min)	4.5	4.5
Gas Exchange Area (m^2)	0.2	1.4
Capillary Blood Volume (ml)	2	13.5
Capillary Pressure Drop (mmHg)	10	10
Capillary Shear Stress (dyn/cm^2)	29	11
Capillary Length (μm)	375	1000
Improved Portability	-	✓
Hemocompatibility Advantage	?	?

The device which utilizes pure oxygen has a much smaller gas exchange area and smaller capillary blood volume. The device using air has a smaller capillary shear stress, a longer capillary length, and would have improved portability due to the elimination of gas cylinders. Which device would have better hemocompatibility is not known. The pure oxygen device provides a much smaller gas exchange surface area and thus less foreign body exposure to the blood. The air device provides more natural ventilation and eliminates the hemocompatibility issues associated with using pure oxygen as the supply gas (see Section B.). Both approaches have advantages over commercially-available devices and may find application in different clinical configurations.

E. History of Microfluidic Artificial Lungs

If a microfluidic artificial lung is defined as an artificial lung with a blood channel height of less than or equal to approximately 100 μm, the first microfluidic artificial lung was developed by Kolobow and Bowman in 1963 [55]. The device consisted of a 127 μm-thick silicone-coated screen membrane that was wrapped around a central cylinder. Blood flowed between the membrane layers in 80 μm-thick "sheets". The 1.2 m^2 device had a priming volume of 110 ml, an oxygen transfer of 82 $ml \bullet m^{-2} \bullet min^{-1}$, and served as the foundation for current commercial silicone-membrane artificial lungs. In the 1977, Hung et al. developed flat-plate membrane oxygenators that contained 110 μm-tall blood channels etched into a stainless steel plate and sandwiched against the same 127 μm-thick silicone-based membrane used by Kolobow [56]. After this early work, research in microfluidic artificial lungs was largely stalled due to the large hydraulic resistance of small diameter blood channels and the advent of hollow fiber membrane technology. Due to their porosity, hollow fiber membranes have very large gas permeabilities and can also be used to create artificial lungs with low hydraulic resistances. For these reasons, devices based on hollow fiber technology became the dominant clinical artificial lung technology and still hold that position today. Due to the large gas permeability of hollow

fiber membranes, the gas exchange of artificial lungs became limited mainly by the diffusional resistance of their blood channels. Other drawbacks of current artificial lungs have already been discussed above.

The explosion of microfluidics and lab-on-a-chip technologies and the promise of increased gas exchange at the micro-scale recently led to increased research interest in microfluidic artificial lungs. In 2004, Federspiel and Svitek predicted that future artificial lung technologies will likely contain "gas exchange units aimed at mimicking the scale and function of the alveolar-capillary units of the natural lung" and with "micron-scale blood channels" in "intimate contact" with gas channels [57].

In 2008, Lee et al. compared various approaches to construct microfluidic artificial lungs and implemented two small-scale prototype designs [58, 59, 60]. One of the designs featured an array of 15 μm-tall blood channels and a 130 μm-thick PDMS gas exchange membrane and was capable of partially oxygenating anticoagulated porcine blood [60]. They predicted that a human-scale version of their design with a blood flow of 4 L/min could have a priming volume as small as 13 ml [60]. This pioneering work was analysed using the equations of Section C in [37]. Theoretical predictions agreed well with experimental results and suggested that the gas exchange of the device was limited by the thickness of the PDMS membrane. The small, single height of the microchannels (15 μm) could result in large pressure drop for a larger area design without other modifications.

In 2009, Burgess et al. presented a small-scale, PDMS artificial lung with 33 μm-tall, semi-circular blood channels and a PDMS gas transfer membrane with a thickness as small as 64 μm [61]. The research group measured gas permeance through their membrane and proposed a method to stack many layers in parallel, although they acknowledged that the process would be labor intensive. They also demonstrated that endothelial cells could be successfully grown in the PDMS microchannels.

In 2009, Potkay presented results for a small-scale, silicone artificial lung with 30 μm-tall artificial capillaries and a 15 μm-thick gas diffusion membrane [62]. The device contained the thinnest silicone membrane to date and was used to oxygenate deionized water. The design of the single-height blood channels in this early work, however, did not take into account shear stress or pressure drop.

In 2010, Hoganson et al. described small-scale microfluidic artificial lungs with a branched vascular network with 200 μm-tall blood microchannels and three different membranes: a 12 μm-thick microporous polycarbonate membrane; a 15 μm-thick silicone-coated polycarbonate membrane; and, and 63 μm-thick non-porous silicone membrane (Fig. 8A) [63]. Their blood channel network had a hydraulic resistance of 15.4 mmHg•ml^{-1}•min and exhibited shear stresses between 1 and 26.6 dyn•cm^{-2} at a flow rate of 4 ml/min. Blood oxygenation for all three membranes was similar, suggesting that gas transfer was limited by diffusion in the blood channel, and was on the same order as commercially-available alternatives (89.3 ml•min^{-1}•m^{-2}). Pure oxygen was used as the supply gas. The equations in

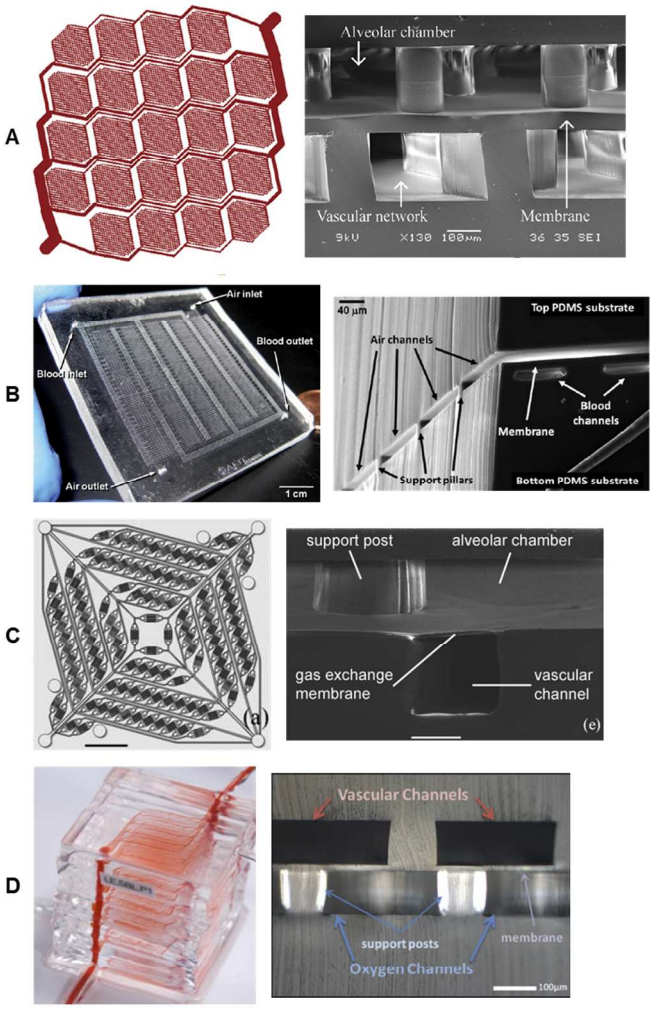

Fig. 8 A sample of the microfluidic artificial lung designs that have been constructed and tested to date. A) Hoganson et al. 2010 [63]; B) Hoganson et al. 2011 [63]; C) Potkay et al. 2011 [33]; D) Kniazeva et al. 2011, 2012 [68, 64].

Section C were used to validate these experimental results in [37]. Theory agreed with experimental results and confirmed that gas exchange was limited by the large height of the blood channels.

In 2011, Potkay et al. presented results for small-scale, all-PDMS microfluidic artificial lungs with 15 μm-thick, non-porous membranes and 20 and 10 μm-tall artificial capillaries (Fig. 8B) [33]. The blood flow network featured blood channels with heights of 140, 60 and 20 or 10 μm to simulate the branching of the natural lung. Most notably, devices tested with whole porcine blood and with air as the supply gas were able to achieve gas exchange efficiencies comparable to commercially-available blood oxygenators that utilize pure oxygen as the supply gas. This result represented a major step toward making truly-portable artificial lungs by eliminating the need for pure oxygen stored in gas cylinders. These results were also the first to verify that microfluidic artificial lungs can have gas exchange efficiencies vastly exceeding those of current hollow-fiber based devices. Finally, Potkay et al. demonstrated the need for improving hemocompatibility of microchannel blood

Table 2 A summary of previous work in microfluidic artificial lungs. Only devices tested with blood are included in the table. Data for the Novalung iLA Membrane Ventilator and the natural lung are given at the bottom of the table for comparison. Gas exchange data represent the maximum values reported. Blood flow is the flow rate at which the maximum oxygen exchange was achieved. PC is nanoporous polycarbonate, μP is microporous, and PP is polypropylene hollow fiber. SAV is surface area to volume ratio.

Source	Blood Channel Height (μm)	Membrane Thickness (μm)	SAV (cm^{-1})	Membrane Material	O_2 Exchange ($ml \bullet min^{-1} \bullet m^{-2}$)	CO_2 Exchange ($ml \bullet min^{-1} \bullet m^{-2}$)	Blood Flow ($L \bullet min^{-1} \bullet m^{-2}$)	Supply Gas
Lee 2008 [60]	15	130	476	PDMS	256	-	22.5	O_2
	15	130	476	PDMS	85	-	9.1	Air
Hoganson 2010 [63]	200	12	50	PC	136	111	4.9	O_2
	200	15	50	PDMS / PC	145	86	4.9	O_2
	200	63	50	PDMS	151	40	4.9	O_2
Potkay 2011 [33]	20	15	400	PDMS	137	346	6.4	Air
	10	15	800	PDMS	225	492	9.0	Air
Hoganson 2011 [27]	100	9	100	PDMS	41	191	9.1	O_2
Kniazeva 2012 [64]	50	30	200	PDMS	329	-	11.7	O_2
	100	30	100	PDMS	317	-	11.7	O_2
	50	117	200	PDMS	223	-	11.7	O_2
Wu 2013 [65]	80	15	125	PDMS	12	108	2.6	Air
	80	15	125	μP PDMS	19	92	2.6	Air
	80	6	125	PC	13	90	2.6	Air
Rochow 2014 [66]	80	20	125	PDMS	104	101	2.6	O_2
	80	20	125	PDMS	31	140	2.6	Air
Novalung iLA [18]	200	30	74	PP	177	154	3.5	O_2
Human lung [8]	10	2	300	Cell	100	100	0.7	Air

networks. Blood side pressure increased significantly over a period of 1 to 3 hours despite the use of heavy anticoagulation. The theoretical model presented in Section C was used to analyze this device. Experimental results agreed very well with theory [37]. Because the artificial capillary height is near the practical minimum (10 μm), the gas exchange performance of the device could only be improved through a thinner or porous membrane or by moving from one to two-sided diffusion. The fluidic design could be improved through tapered microchannels and branching angles that more closely follow Murray's law, thereby providing more constant flow and shear stress throughout the device.

In 2011, Hoganson et al. presented a small-scale microfluidic lung assist device which contained 100 μm-tall, rectangular blood channels, a 9 μm-thick gas transfer membrane, and a blood channel network with physiological blood flow (Fig. 8C) [27]. Particularly of note in this design is that fact that the blood channel network was designed to follow natural branching and scaling laws as described by Murray in 1926 [45, 46]. Microchannels were further designed to have uniform flow at bifurcations, biomimetic vessel length, and shear stress between 14 and 56 $dyn \bullet cm^{-2}$, or within the physiologic arterial range. Oxygen exchange efficiency was 41 $ml \bullet min^{-1} \bullet m^{-2}$ while using oxygen as the supply gas. The use of a single blood channel height simplifies device construction and should reduce clotting (due to its large height relative to the diameter of a blood cell). However, the modeling of Section C demonstrates that the gas exchange efficiency could be significantly increased if the blood channel height is reduced.

Also in 2011, the same research group published a paper that investigated the impact of channel size, oxygen exposure length and blood shear rate on gas exchange in a small-scale microfluidic artificial lung [67]. In the study, artificial capillaries with dimensions of 50 x 50, 100 x 100, and 150 x 150 μm were tested in conjunction with a 9.5 μm-thick silicone membrane. The researchers found that gas transfer increased with flow rate blood oxygen saturation was found to be inversely related to flow rate per channel. Tests were performed at very high blood flow rates (up to 400 $L \bullet min^{-1} \bullet m^{-2}$) compared to current commercial blood oxygenators (up to 4 $L \bullet min^{-1} \bullet m^{-2}$) thereby slightly decreasing the relevance of the experimental data.

In 2011, Kniazeva et al. developed a small-scale microfluidic artificial lung with a branching architecture with uniform shear, 100 μm-tall blood channels, and an 11 μm-thick gas transfer membrane (Fig. 8D) [68]. They additionally developed a method to stack multiple devices together in parallel. In a later paper in 2012, they measured the impact of combining up to ten of their devices in parallel through tests with whole bovine blood [64]. Devices with blood channel heights of 50 and 100 μm and membrane thicknesses (silicone) of 30 and 117 μm were tested. In general, increasing the number of layers, decreasing membrane thickness, and decreasing blood channel height were found to increased gas transfer. Furthermore, decreasing the blood channel height resulted in a large decrease in blood priming volume. Similar to other previous work, the choice of a constant, releatively large blood channel height simplified device construction and likely will help decrease thrombosis. However, decreasing the height of their gas exchange, blood flow microchannels would significantly increase gas exchange efficiency.

In 2011 and 2013, Wu et al. presented results for a small-scale microfluidic blood oxygenator targeted at lung assist in newborn infants [69, 65]. A silicone device containing 80 μm-high blood channels was tested with non-porous and microporous 15 μm-thick silicone membranes and 6 μm-thick

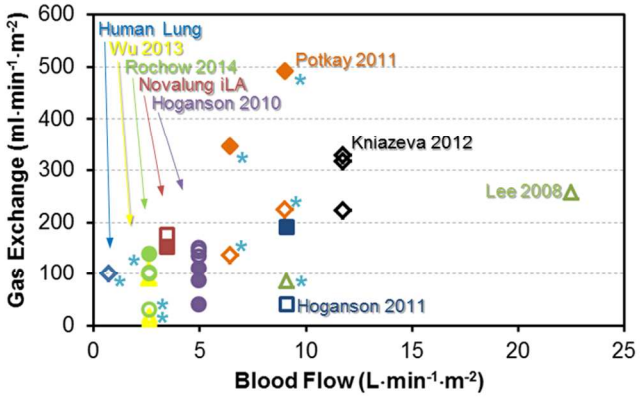

Fig. 9 A graphical summary of the gas exchange of microfluidic artificial lungs to date from Table 2. Data points from the same publication have the same shape and color. Open shapes represent O_2 exchange. Filled shapes represent CO_2 exchange. Data collected using air as the sweep gas are marked with an asterisk (*).

porous polycarbonate membranes. The device structure was unique in that the gas side of the membrane was directly exposed to air. Although this technique simplifies the construction of single-layer devices, it also increases the risk of a membrane rupture. Elevated blood side pressures due to clotting could lead to significant membrane deflection and possible failure. Devices with porous silicone membranes exhibited an oxygen exchange efficiency approximately 15 $ml \bullet min^{-1} \bullet m^{-2}$ with oxygen as the supply gas. This oxygen exchange is less than half of that predicted by the equations in Section C. This may be due to difference between theoretical and experimental parameters (no blood hematocrit was reported) or due to the fact that oxygen must diffuse to the open gas-side surface of the membrane.

In 2012 and 2014, the same research group led by Rochow et al. stacked their small-scale microfluidic oxygenator in parallel and tested them *in vitro* and *in vivo* [70, 66]. A custom-designed 3D-printed manifold was used to combine up to 14 devices together. A 10 oxygenator manifold had a priming volume of 4.8 ml and was designed to supplement the respiratory function of a 1 kg infant. For the *in vivo* experiments, the 10-device stack was attached between the umbilical artery and vein in two anesthetized newborn piglet. Blood flow was driven by the natural pressure and *in vivo* oxygen exchange was 30 $ml \bullet min^{-1} \bullet m^{-2}$ at a blood flow rate of up to 1.6 $L \bullet min^{-1} \bullet m^{-2}$. Details of clotting and lifetime during the *in vivo* experiments were not reported.

To date, various small-scale microfluidic artificial lung designs have been constructed and tested (Fig. 8). In summary, microfluidic artificial lungs have been developed with gas exchange efficiencies, surface-area-to-volume ratio, and blood priming volumes that are vastly superior to current commercially-available alternatives as well as blood flow networks with more uniform, physiologic flow and hydraulic resistances compatible with natural pressures. Table 2 and Fig. 9 provide performance comparisons of microfluidic artificial lung work to date.

E.1. Previous work on improving the long-term hemocompatibility of microchannels

Although there have been many works describing improving the biocompatibility of materials including PDMS [52, 53, 54], to date there are only several works that specifically have looked at improving the long-term hemocompatibility of blood transporting microchannel networks. As described previously, this is a major issue for microchannels, where if the coagulation process is started, it will take a relatively small number of cells to block a micron-scale blood channel.

In 2013, Zhang et al. modified the surface of 350 x 600 μm rectangular PDMS microchannels with polybetaine and investigated its effect on thrombus formation [34]. In this work, polybetaine was deposited on the surface of PDMS to a thickness of 1 to 2 μm using surface-initiated polymerization of sulfobetaine monomer. The coating reduced the contact angle of the surface from 114.9° (uncoated PDMS) to 20.8° (coated PDMS) and reduced fibrinogen adsorption by 96% compared to uncoated controls. Devices were then tested with heparinized (0.5 U/ml) whole bovine blood at a flow rate of 1.7 ml/min (shear rate of 400 s^{-1} or approximately 8 dyn/cm^2) for up to one hour. All uncoated devices formed occlusive thrombi in less than one hour. Polybetaine modified devices, on the other hand, exhibited a 5 to 10 fold decrease in thrombus formation in the microchannels and exhibited minimal pressure increase over the one hour testing duration. Longer time frames and application to smaller microchannels were not tested in this study.

In 2014, Kovach et al. modified the surface of microchannel networks with polyethylene glycol (PEG) and investigated its effect on hemocompatibility [35]. In this work, PEG was grafted to the surface of the PDMS microchannels using plasma-assisted surface modification. The surface modification immediately reduced the contact angle of PDMS from 105° to 5°. Over time, the contact angle of the PEG-modified surface gradually increased and stabilized at 25° (~10 days). PEG-grafted surfaces significantly decreased fibrinogen adsorption up to 28 days after coating, highlighting the stability and functionality of the coating over time, and decreased platelet adhesion by a factor of 50. Complex microchannel networks containing 225, 60, and 20 μm-tall blood channels were then modified with PEG and tested with heparinized (6.7 U/ml) whole porcine blood at 0.7 ml/min (shear stress of 5 dyn/cm^2) for up to 19 hours. The pressure across coated microchannel networks took over 16 times longer to double than the uncoated controls and exhibited significantly less surface-bound clots despite being tested under blood flow for 25 times longer.

Other researchers have attempted to line the walls of microchannels with endothelial cells in order to mimic the natural vasculature [71, 72, 73, 74]. In 2002, Borenstein et al. pioneered this area by seeding a confluent monolayer of endothelial cells into microfluidic channels down to 30 μm in diameter [71, 72]. Specifically related to microfluidic artificial lungs, in 2009, Burgess et al. lined the surface of blood channels in a microfluidic artificial lung with endothelial cells

in an effort to provide a non-thrombogenic surface and reduce the need for systemic anticoagulation during treatment with artificial lungs [61]. They successfully cultured confluent and viable monolayers of endothelial cells in the microchannels after 10 days of perfusion. However, no blood compatibility or lifetime studies were presented. In 2010, Polk et al. coated the outer surface of a hollow-fiber membrane artificial lung with a confluent layer of endothelial cells and tested for thrombotic deposition and gas exchange [75]. Endothelialized membranes displayed significantly less thrombosis area (more than a factor of two less) than uncoated controls in acute tests, but also displayed a decreased gas exchange rate. More recent studies have demonstrated that endothelial cells can survive for up to 37 days in a microchannel environment [76].

F. Future Challenges for Microfluidic Artificial Lungs

In order for microfluidic artificial lungs to become a clinical reality, two main hurdles will have to be overcome related to: 1) large-scale manufacturing, and 2) long-term hemocompatibility. These two challenges are discussed below.

F.1. Large scale integration and manufacturing

Small-scale microfluidic artificial lungs have exhibited gas exchange efficiencies vastly exceeding those of their conventional counterparts [33, 64]. Each of these small-scale microfluidic artificial lungs has thus far been formed from a single blood and single gas layer separated by a gas diffusion membrane. Despite their efficiency, hundreds to thousands of these small-scale, single-layer microfluidic artificial lungs would be required to provide pulmonary support at a level comparable to current clinical artificial lungs [33, 58, 61, 63]. Researchers have combined up to 14 single layer devices together using custom manifolds [64, 70, 66]. However, the feasibility of extending this technique to hundreds or thousands of devices is unknown and challenging.

It is thus likely that new manufacturing technologies will need to be developed that can create a large, multi-layer array of tightly packed microchannels. Figure 1 demonstrates this concept. These next generation, large-scale microfluidic artificial lungs will likely need to have many closely-packed blood and gas layers separated by gas diffusion membranes (right in Fig. 1). To be cost effective, the developed manufacturing techniques will likely need to be both simple and automated.

Although a manufacturing technology capable of creating the structure in Fig. 1 does not yet exist, past approaches may provide ideas for possible solutions. In 1963, Kolobow and Bowman presented an artificial lung in which a 127 μm-thick silicone membrane was wrapped around a central cylinder [55]. This idea could be leveraged to wrap a large-area, single-layer, microfluidic artificial lung around a cylindrical substrate. This approach would potentially be compact and simple to manufacture, but vertical feedthroughs would be required to reduce pressure drops.

Other previous work [77, 78] described a membrane oxygenator that was formed from a silicone sheet that was folded back and forth around spacers, resulting in an accordion-like final structure. This folding technique could potentially be applied to generate a multi-layer, stacked, and compact large-scale microfluidic artificial lung.

Finally, the techniques already developed by research groups [64, 70, 66] to stack single layer devices (Fig. 8D) may provide a solution through further development. With continued advancement, it is possible that this approach could result in a compact, large-area device.

F.2. Long-term hemocompatibility

Researchers have demonstrated that the surface of microchannels can modified in order to provide improved hemocompatibility [34, 35]. However, device lifetimes greater than one day have not yet been demonstrated. Others have demonstrated microchannel geometries and networks that closely mimic their natural counterparts in terms of branching and shear stress [27, 33]. However, their impact on blood compatibility has not yet been quantified. Microfluidic artificial lungs, in their current form, are likely only applicable for clinical applications requiring a lifetime measured in hours (e.g. cardiopulmonary bypass procedures). However, most clinical applications require artificial lung lifetimes between one day (i.e. acute lung disease) to several months (i.e. chronic lung disease or lung failure). To date, microfluidic artificial lungs have not demonstrated this level of hemocompatibility.

Microfluidic artificial lungs for long-term application will need to contain blood flow networks that minimize the foreign body response. Cells and platelets in these flow networks should experience shear stresses in physiologic range in order to avoid platelet activation and thrombus initiation [24, 25, 26, 27, 79]. One potential approach is thus to design blood flow networks that closely mimic their natural counterpart [27, 68]. Such microchannel networks would follow natural scaling and branching laws [45, 46], exhibit flow velocities and shear stress similar to those in the natural vasculature, and provide additional strategies to reduce protein adhesion, platelet activation, inflammation, and thrombosis. These additional strategies may include surface modifications, careful blood channel design, and potentially the use of endothelial cells to line the wall of the microchannels. Finally, the hemocompatibility and gas exchange of large area microfluidic artificial lungs will need to be validated in animal models and clinical trials.

G. Conclusions

Artificial lungs with micron-scale blood channels and membranes potentially offer significant advantages in terms of gas exchange, portability, and biocompatibility compared to current alternatives. Microfluidic artificial lungs promise to drastically reduce surface area and priming volume (to improve patient outcomes and reduce device size), provide more natural blood flow paths (to improve hemocompatibility), and enable

more natural ventilation (through the use of air instead of pure oxygen). Although significant challenges remain before they can be used clinically, microfluidic artificial lungs thus have the potential to revolutionize the treatment and rehabilitation of lung-disease patients through the development of the first truly-portable, hemocompatible blood oxygenators.

Acknowledgements

I would like to thank Mr. Kyle Kovach for providing advice and feedback regarding this manuscript. This work was supported by Department of Veterans Affairs Rehabilitation Research and Development (VA RR&D) Grant F7404-R and VA RR&D Grant C3819C, The Advanced Platform Technology Research Center of Excellence.

Notes and references

[a] VA Ann Arbor Healthcare System, Ann Arbor, MI 48105 USA
Department of Surgery, University of Michigan, Ann Arbor, MI 48109 USA
Department of Electrical Engineering and Computer Science, Case Western Reserve University, Cleveland, OH 44106 USA
E-mail: jpotkay@umich.edu

Electronic Supplementary Information (ESI) available: [details of any supplementary information available should be included here]. See DOI: 10.1039/b000000x/

Citations

[1] World Health Organization, February 2014. [Online]. Available: http://www.who.int/respiratory/en/.

[2] American Lung Association, 09 2011. [Online]. Available: http://www.lungusa.org/about-us/publications/.

[3] G. Matheis, "New technologies for respiratory assist," *Perfusion,* vol. 18, pp. 245-251, 2003.

[4] G. J. Peek, M. Mugford, R. Tiruvoipati, A. Wilson, E. Allen, M. M. Thalanany, C. L. Hibbert, A. Truesdale, F. Clemens, N. Cooper, R. K. Firmin and D. Elbourne, "Efficacy and economic assessment of conventional ventilatory support versus extracorporeal membrane oxygenation for severe adult respiratory failure (CESAR): a multicentre randomised controlled trial," *The Lancet,* vol. 374, pp. 1351-1363, 2009.

[5] J. B. Zwischenberger, S. A. Conrad, S. K. Alpard, L. R. Grier and A. Bidani, "Percutaneous extracorporeal arteriovenous CO2 removal for severe respiratory failure," *Annal. Thorac. Surg.,* vol. 68, no. 1, pp. 181-187, 1999.

[6] S. A. Conrad, A. Bagley, B. Bagley and R. N. Schaap, "Major findings from the clinical trials of the intravascular oxygenator," *Artif Organs,* vol. 18, no. 11, pp. 846-863, Nov 1994.

[7] A. Davies, D. Jones, M. Bailey, J. Beca, R. Bellomo, N. Blackwell, P. Forrest, D. Gattas, E. Granger, R. Herkes, A. Jackson, S. McGuinness, P. Nair, V. Pellegrino, V. Pettilä, B. Plunkett, R. Pye, P. Torzillo, S. Webb, M. Wilson and M. Ziegenfuss, "Extracorporeal Membrane Oxygenation for 2009 Influenza A(H1N1) Acute Respiratory Distress Syndrome," *JAMA,* vol. 302, pp. 1888-1895, 2009.

[8] W. J. Federspiel and K. A. Henchir, "Lung, Artificial: Basic Principles and Current Applications," in *Encyclopedia of Biomaterials and Biomedical Engineering*, G. L. Bowlin and G. Wnek, Eds., New York, Marcel Dekker, 2004, pp. 910-921.

[9] Maquet Holding B.V & Co., "Quadrox-i Adult and Small Adult," 2014. [Online]. Available: http://www.maquet.com/in/product/QUADROX-i-Adult-and-Small-Adult. [Accessed 29 05 2014].

[10] A. Thiara, V. Høyland, H. Norum, T. Aasmundstad, H. Karlsen, A. Fiane and O. Geiran, "Extracorporeal membrane oxygenation support for 59 days without changing the ECMO circuit: a case of Legionella pneumonia," *Perfusion,* vol. 24, no. 1, pp. 45-7, 2009.

[11] A. A. Mangi, D. P. Mason, J. J. Yun, S. C. Murthy and G. B. Pettersson, "Bridge to lung transplantation using short-term ambulatory extracorporeal membrane oxygenation," *The Journal of Thoracic and Cardiovascular Surgery,* vol. 140, no. 3, pp. 713-715, 2010.

[12] J. P. Garcia, Z. N. Kon, C. Evans, Z. Wu, A. T. Iacono, B. McCormick and B. P. Griffith, "Ambulatory veno-venous extracorporeal membrane oxygenation: Innovation and pitfalls," *The Journal of Thoracic and Cardiovascular Surgery,* vol. 142, no. 4, pp. 755-761, 2011.

[13] D. Hayes, J. Kukreja, J. D. Tobias, H. .. Ballard and C. W. Hoopes, "Ambulatory venovenous extracorporeal respiratory support as a bridge for cystic fibrosis patients to emergent lung transplantation," *Journal of Cystic Fibrosis,* vol. 11, no. 1, pp. 40-45, 2012.

[14] O. M. Shapira, G. S. Aldea, P. R. Treanor, R. M. Chartrand, K. M. DeAndrade, H. L. Lazar and R. J. Shemin, "Reduction of allogeneic blood transfusions after open heart operations by lowering cardiopulmonary bypass prime volume," *The Annals of Thoracic Surgery,* vol. 65, no. 3, pp. 724-730, 1998.

[15] P. G. Jansen, H. te Velthuis, E. R. Bulder, R. Paulus, M. R. Scheltinga, L. Eijsman and C. R. Wildevuur, "Reduction in prime volume attenuates the hyperdynamic response after cardiopulmonary bypass," *The Annals of thoracic surgery,* vol. 60, no. 3, pp. 544-545, 1995.

[16] J. E. Cormack, R. J. Forest, R. C. Groom and J. Morton, "Size makes a difference: use of a low-prime cardiopulmonary bypass circuit and autologous priming in small adults," *Perfusion,* vol. 15, no. 2, pp. 129-135, 2000.

[17] Medtronic, Inc., February 2014. [Online]. Available: http://www.medtronic.com/for-healthcare-professionals/products-therapies/cardiovascular/cardiopulmonary-products/affinity-nt-cardiotomy-venous-reservoir/.

[18] Novalung GMBH, February 2014. [Online]. Available: http://www.novalung.com/en_products_and_services_membrane_ventilators_ila.html.

[19] Terumo Cardiovascular Group, "CAPIOX RX Oxygenators," [Online]. Available: http://www.terumo-cvs.com/products/ProductDetail.aspx?groupId=1&familyID=1&country=1. [Accessed 6 February 2014].

[20] D. S. Lawson, R. Ing, I. M. Cheifetz, R. Walczak, D. Craig, S. Schulman, F. Kern, I. R. Shearer, A. Lodge and J. Jaggers, "Hemolytic characteristics of three commercially available centrifugal blood pumps," *Pediatric Critical Care Medicine,* vol. 6, no. 5, pp. 573-577, September 2005.

[21] R. E. Schewe, K. M. Khanafer, A. Arab, J. A. Mitchell, D. J. Skoog and K. E. Cook, "Design and In Vitro Assessment of an Improved, Low-Resistance Compliant Thoracic Artificial Lung," *ASAIO Journal,* vol. 58, no. 6, p. 583–589, November/December 2012.

[22] S. Chambers, S. Merz, J. McGillicuddy and R. Bartlett, "Development of the MC3 BioLung," in *Proceedings of the 24th Annual Conference of the Engineering in Medicine and Biology Society and the Annual Fall Meeting of the Biomedical Engineering Society Conference*, Houston, TX, 2002.

[23] J. E. Hall, Guyton and Hall Textbook of Medical Physiology, 12th ed., Philadelphia, PA: Saunders, 2011.

[24] A. M. Malek, S. L. Alper and S. Izumo, "Hemodynamic Shear Stress and Its Role in Atherosclerosis," *JAMA,* vol. 282, no. 21, pp. 2035-2042, 1999.

[25] P. Reinhard, J. Apel, S. Klaus, F. Schügner, P. Schwindke and H. Reul, "Shear Stress Related Blood Damage in Laminar

Couette Flow," *Artificial Organs,* vol. 27, no. 6, pp. 1525-1594, 2003.

[26] Y. Ikeda, M. Handa, K. Kawano, T. Kamata, M. Murata, Y. Araki, H. Anbo, Y. Kawai, K. Watanabe and I. Itagaki, "The role of von Willebrand factor and fibrinogen in platelet aggregation under varying shear stress," *J Clin Invest,* vol. 87, no. 4, pp. 1234-1240, 1991.

[27] D. M. Hoganson, H. I. Pryor II, E. K. Bassett, I. D. Spool and J. P. Vacanti, "Lung assist device technology with physiologic blood flow developed on a tissue engineered scaffold platform," *Lab on a Chip,* vol. 11, no. 4, pp. 700-707, 2011.

[28] J. T. Borenstein, E. J. Weinberg, B. K. Orrick, C. Sundback, M. R. Kaazempur-Mofrad and J. P. Vacanti, "Microfabrication of three-Dimensional engineered scaffolds," *Tissue Engineering,* vol. 13, no. 8, pp. 1837-1844, 2007.

[29] N. G. LaFayette, R. E. Schewe, J. P. Montoya and K. E. Cook, "Performance of a MedArray Silicone Hollow Fiber Oxygenator," *ASAIO Journal,* vol. 55, no. 4, pp. 382-387, 2009.

[30] M. Hirthler, J. Simoni and M. Dickson, "Elevated levels of endotoxin, oxygen-derived free radicals, and cytokines during extracorporeal membrane oxygenation," *J Pediatr Surg,* vol. 27, no. 9, pp. 1199-1202, 1992.

[31] P. J. Marro, S. Baumgart, M. Delivoria-Papadopoulos, S. Zirin, L. Corcoran, S. P. McGaurn, L. E. Davis and R. R. Clancy, "Purine Metabolism and Inhibition of Xanthine Oxidase in Severely Hypoxic Neonates Going onto Extracorporeal Membrane Oxygenation," *Pediatric Research,* vol. 41, no. 4, p. 513–520, 1997.

[32] R. A. Hayes, K. Shekar and J. F. Fraser, "Is hyperoxaemia helping or hurting patients during extracorporeal membrane oxygenation? Review of a complex problem," *Perfusion,* vol. 28, no. 3, pp. 184-193, 2013.

[33] J. Potkay, M. Magnetta, A. Vinson and B. Cmolik, "Bio-inspired, efficient, artificial lung employing air as the ventilating gas," *Lab on a Chip,* vol. DOI: 10.1039/c11c20020h, 2011.

[34] Z. Zhang, J. Borenstein, L. Guiney, R. Miller, S. Sukavaneshvar and C. Loose, "Polybetaine modification of PDMS microfluidic devices to resist thrombus formation in whole blood," *Lab on a Chip,* vol. 13, no. 10, pp. 1963-1968, 2013.

[35] K. M. Kovach, J. R. Capadona, A. S. Gupta and J. A. Potkay, "The effects of PEG-based surface modification of PDMS microchannels on long-term hemocompatibility," *Journal of Biomedical Materials Research Part A,* 2014.

[36] U.S. Department of Health and Human Services Food and Drug Administration, "Guidance for Cardiopulmonary Bypass Oxygenators 510(k) Submissions; Final Guidance for Industry and FDA Staff," November 2000. [Online]. Available: http://www.fda.gov/MedicalDevices/DeviceRegulationandGuidance/GuidanceDocuments/ucm073668.htm.

[37] J. A. Potkay, "A simple, closed-form, mathematical model for gas exchange in microchannel artificial lungs," *Biomedical Microdevices,* vol. 15, no. 3, pp. 397-406, Jan 2013.

[38] A. V. Hill, "The possible effects of the aggregation of the molecules of haemoglobin on its dissociation curves," *J Physiol,* vol. 40, pp. 4-7, 1910.

[39] M. L. Turgeon, Clinical Hematology: Theory and Procedures, 4th ed., Baltimore, MD: Lippincott Williams & Wilkins, 2004.

[40] B. Alberts, A. Johnson, J. Lewis, M. Raff, K. Roberts and P. Walter, Molecular Biology of the Cell, 4th ed., New York: Garland Science, 2002.

[41] N. A. Campbell, J. B. Reece, L. A. Urry, M. L. Cain, S. A. Wasserman, P. V. Minorsky and R. B. Jackson, Biology, 8th ed., London: Pearson Education.

[42] D. Braasch, "Red cell deformability and capillary blood flow," *Physiological Reviews,* vol. 51, no. 4, pp. 679-701, October 1971.

[43] E. R. Weibel, The pathway for oxygen: structure and function in the mammalian respiratory system, Cambridge: Harvard University Press, 1984.

[44] Dow Corning, June 2014. [Online]. Available: http://www.dowcorning.com/applications/search/products/Details.aspx?prod=01064291.

[45] C. D. Murray, "The physiological principle of minimum work. I. The vascular system and the cost of blood volume," *Proceedings of the National Acadamy of Sciences,* vol. 12, no. 3, pp. 207-214, 1926.

[46] C. D. Murray, "The physiological principle of minimum work applied to the angle of branching of arteries," *The Journal of General Physiology,* vol. 9, no. 6, pp. 835-841, 1926.

[47] M. Zamir, "Optimality Principles in Arterial Branching," *Journal of Theoretical Biology,* vol. 62, no. 1, pp. 227-251, 1976.

[48] T. F. Sherman, "On connecting large vessels to small. The meaning of Murray's law.," *Journal of General Physiology,* vol. 78, no. 4, pp. 431-453, 1981.

[49] R. Revellin, F. Rousset, D. Baud and J. Bonjour, "Extension of Murray's law using a non-Newtonian model of blood flow," *Theoretical Biology and Medical Modelling,* vol. 6, no. 7, 2009.

[50] A. Zimmermann, H. Aebert, A. Reiz, M. Freitag, M. Husseini, G. Ziemer and H. Wendel, "Hemocompatibility of PMEA coated oxygenators used for extracorporeal circulation procedures," *ASAIO Journal,* vol. 50, no. 3, pp. 193-9, 2004.

[51] H. Wendel and G. Ziemer, "Coating-techniques to improve the hemocompatibility of artificial devices used for extracorporeal circulation," *European Journal Cardio-Thoracic Surgery,* vol. 16, no. 3, pp. 342-50, 1999.

[52] J. Goddard and J. Hotchkiss, "Polymer surface modification for the attachment of bioactive compounds," *Progress in Polymer Science,* vol. 32, no. 7, p. 698–725, 2007.

[53] I. Wong and C. Ho, "Surface molecular property modifications for poly(dimethylsiloxane) (PDMS) based microfluidic devices," *Microfluid Nanofluidics,* vol. 7, no. 3, pp. 291-306, 2009.

[54] J. Zhou, A. Ellis and N. Voelcker, "Recent developments in PDMS surface modification for microfluidic devices," *Electrophoresis,* vol. 31, no. 1, pp. 2-16, 2010.

[55] T. Kolobow and R. L. Bowman, "Construction and Evaluation of An Alveolar Membrane Artificial Heart-Lung," *ASAIO Journal,* vol. 9, no. 1, pp. 238-243, 1963.

[56] T.-K. Hung, H. S. Borovetz and M. H. Weissman, "Transport and flow phenomena in a microchannel membrane oxygenator," *Annals of Biomedical Engineering,* vol. 5, no. 4, pp. 343-361, 1977.

[57] W. J. Federspiel and R. G. Svitek, "Lung, Artificial: Current Research and Future Directions," in *Encyclopedia of Biomaterials and Biomedical Engineering*, New York, Marcel Dekker, Inc., 2004, pp. 922-931.

[58] J. K. Lee and H. H. M. L. F. Kung, "Microchannel Technologies for Artificial Lungs: (1) Theory," *ASAIO Journal,* vol. 54, no. 4, pp. 372-382, 2008.

[59] M. C. Kung, J. K. Lee and H. H. M. L. F. Kung, "Microchannel Technologies for Artificial Lungs: (2) Screen-filled Wide Rectangular Channels," *ASAIO Journal,* vol. 54, no. 4, pp. 383-9, 2008.

[60] J. Lee, M. Kung, H. Kung and L. Mockros, "Microchannel technologies for artificial lungs:(3) open rectangular channels," *ASAIO journal,* vol. 54, no. 4, pp. 390-395, 2008.

[61] K. Burgess, H. Hu, W. Wagner and W. Federspiel, "Towards microfabricated biohybrid artificial lung modules for chronic respiratory support," *Biomedical microdevices,* vol. 11, no. 1, pp. 117-127, 2009.

[62] J. A. Potkay, "A high efficiency micromachine artificial lung," *The 15th International Conference on Solid-State Sensors, Actuators and Microsystems (Transducers 2009),* pp. 2234-2237, June

2009.

[63] D. Hoganson, J. Anderson, E. Weinberg, E. Swart, B. Orrick, J. Borenstein and J. Vacanti, "Branched vascular network architecture: a new approach to lung assist device technology," *General Thoracic Surgery,* vol. 140, no. 5, pp. 990-5, 2010.

[64] T. Kniazeva, A. A. Epshteyn, J. C. Hsiao, E. S. Kim, V. B. Kolachalama, J. L. Charest and J. T. Borenstein, "Performance and scaling effects in a multilayer microfluidic extracorporeal lung oxygenation device," *Lab on a Chip,* vol. 12, pp. 1686-1695, 2012.

[65] W. Wu, N. Rochow, E. Chan, A. Manan, C. Fusch, D. Nagpal, P. R. Selvaganapathy and G. Fusch, "Lung assist device: development of microfluidic oxygenators for preterm infants with respiratory failure," *Lab on a Chip,* vol. 13, pp. 2641-2650, 2013.

[66] N. Rochow, A. Manan, W. I. Wu, G. Fusch, S. Monkman, J. Leung, E. Chan, D. Nagpal, D. Predescu, J. Brash and C. Fusch, "An Integrated Array of Microfluidic Oxygenators as a Neonatal Lung Assist Device: In Vitro Characterization and In Vivo Demonstration," *Artificial Organs,* 2014.

[67] E. Bassett, D. Hoganson, J. Lo, E. Penson and J. Vacanti, "Influence of vascular network design on gas transfer in lung assist device technology," *ASAIO Journal,* vol. 57, no. 6, pp. 533-8, 2011.

[68] T. Kniazeva, J. Hsiao, J. Charest and J. Borenstein, "A microfluidic respiratory assist device with high gas permeance for artificial lung applications," *Biomedical Microdevices,* vol. 13, no. 2, pp. 315-323, 2011.

[69] W. Wu, N. Rochow, G. Fusch, R. Kusdaya, A. Choi, P. R. Selvaganapathy and C. Fusch, "Development of microfluidic oxygenators as lung assisting devices for preterm infants," in *The 15th International Conference on Miniaturized Systems for Chemis*, 2011.

[70] N. Rochow, W. I. Wu, E. Chan, D. Nagpal, G. Fusch, P. R. Selvaganapathy, S. Monkman and C. Fusch, "Integrated microfluidic oxygenator bundles for blood gas exchange in premature infants," in *2012 IEEE 25th International Conference on Micro Electro Mechanical Systems (MEMS)*, 2012.

[71] J. Borenstein, H. Terai, K. King, E. Weinberg, M. Kaazempur-Mofrad and J. Vacanti, "Microfabrication technology for vascularized tissue engineering," *Biomedical Microdevices,* vol. 4, no. 3, p. 167–175, 2002.

[72] J. Borenstein, E. Weinberg, M. Kaazempur-Mofrad and J. Vacanti, "Tissue engineering of microvascular networks," in *Encyclopedia of Biomaterials and Biomedical Engineering*, Marcel Dekker, 2004, p. 1594–1603.

[73] M. Shin, K. Matsuda, O. Ishii, H. Terai, M. Kaazempur-Mofrad, J. Borenstein, M. Detmar and J. Vacanti, "Endothelialized networks with a vascular geometry in microfabricated poly(dimethyl siloxane)," *Biomedical Microdevices,* vol. 6, no. 4, pp. 269-278, 2004.

[74] G. Wang, Y. Hsu, S. Hsu and R. Horng, "JSR photolithography based microvessel scaffold fabrication and cell seeding," *Biomedical Microdevices,* vol. 8, pp. 17-23, 2006.

[75] A. Polk, T. Maul, D. McKeel, T. Snyder, C. Lehocky, B. Pitt, D. Stolz, W. Federspiel and W. Wagner, "A biohybrid artificial lung prototype with active mixing of endothelialized microporous hollow fibers," *Biotechnology and Bioengineering,* vol. 106, no. 3, pp. 490-500, 2010.

[76] I. Voiculescua, F. Lib, F. Liua, X. Zhanga, L. M. Cancelc, J. M. Tarbellc and A. Khademhosseinid, "Study of long-term viability of endothelial cells for lab-on-a-chip devices," *Sensors and Actuators B: Chemical,* vol. 182, pp. 696-705, 2013.

[77] M. Douglas, D. Birnbaum and B. Eiseman, "Biological Evaluation of a Disposable Membrane Oxygenator," *Arch Surg,* vol. 103, no. 1, pp. 89-92, 1971.

[78] T. M. Gordon, R. L. Stewart and D. J. Wellington, "Membrane medical device". USA Patent US4663125 A, May 17 1985.

[79] L. F. Mockros and K. E. Cook, "Engineering Design of Thoracic Artificial Lungs," in *The Artificial Lung*, S. N. Vaslef and R. W. Anderson, Eds., Austin, TX, Landes Biosciences Publishers, 2002, pp. 33-64.

[80] Encyclopaedia Britannica Inc., "pulmonary alveolus," 2014. [Online]. Available: http://www.britannica.com/EBchecked/topic/483141/pulmonary-alveolus. [Accessed 6 February 2014].

